THE JOURNAL OF PHYSICAL CHEMISTRY B

Article

pubs.acs.org/JPCB

Performance of Homeostatic Controller Motifs Dealing with Perturbations of Rapid Growth and Depletion

Gunhild Fjeld,[†] Kristian Thorsen,[‡] Tormod Drengstig,[‡] and Peter Ruoff*[,†]

[†]Centre for Organelle Research and [‡]Department of Electrical Engineering and Computer Science, University of Stavanger, Stavanger 4036, Norway

Supporting Information

ABSTRACT: An essential property of life is that cells and organisms have the ability to protect themselves against external disturbances/attacks by using homeostatic mechanisms. These defending mechanisms are based on negative feedback regulation and often contain additional features, such as integral control, where the integrated error between a controlled variable and its set-point is used to achieve homeostasis. Although the concept of integral control has its origin in industrial processes, recent findings suggest that biological systems are also capable of showing integral control. We recently described a basic set of negative feedback structures (controller motifs) where robust homeostasis is achieved against different but constant perturbations. As many perturbations in biology, such as infections, increase rapidly over time, we investigated how the different controller motifs equipped with different implementations of integral control perform in relation to rapidly changing perturbations, including exponential and hyperbolic changes. The findings show that the construction of an optimum biochemical controller design for time-dependent perturbations requires a certain match between the structure of the negative feedback loop, its signaling kinetics, and the kinetics of how integral control is implemented within the negative feedback loop.

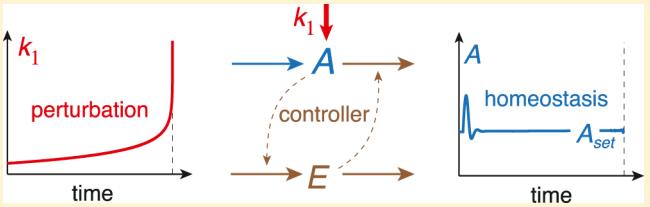

INTRODUCTION

Cannon[1,2] defined the term *homeostasis* as the physiological conditions that keep the concentrations of certain substances within narrow limits.[3] Homeostasis is essential for maintaining the internal stability of cells and organisms and to help them in defending against environmental and internal disturbances. Many aspects of homeostatic regulation have become apparent, such as its involvement in coping with stress,[4,5] its participation in circadian rhythms,[6−8] the involvement of processes that act in a concerted manner,[9−11] and the nonlinear dynamics of defending mechanisms.[12] With the development of cybernetics[13,14] and control engineering[15] the basic regulatory elements of homeostasis have been identified as negative feedback mechanisms.[16]

Figure 1 shows eight basic negative feedback loops (motifs) between a controlled variable A and a controller species E.[17] The motifs divide into two classes, which have been termed *inflow controllers* and *outflow controllers*. Inflow controllers compensate for outflow perturbations in A by adding A to the system (from an external or internal source), whereas outflow controllers remove A from the system into external or internal reservoirs. The reason for this division between inflow and outflow controllers is that the $E_{i,o}$'s can only have positive values (concentrations) and therefore two distinct classes of mechanisms are necessary to add or remove A by $E_{i,o}$. The eight motifs differ in how the signaling from A to $E_{i,o}$ and from $E_{i,o}$ to A occurs, which can be either in the form of activating or inhibitory mechanisms.

One of the mechanisms to achieve robust homeostasis is integral control.[15] Figure 2a illustrates how integral control as part of a negative feedback loop is achieved. In integral control, the deviation/error $\epsilon = A_{set} - A$ between the set-point A_{set} and the value of a controlled variable, A, is integrated. The integrated error E represents the sum of all deviations of A from A_{set} over time and allows compensation for these deviations such that A can precisely reach A_{set}.[15] It further corresponds to the concentrations $E_{i,o}$ in the different controller motifs. Although integral control was invented for industrial processes, such as in the maneuvering of ships, it is now clear that the robustness of biological feedback mechanisms can also be addressed in terms of integral control.[17−29]

To implement integral control within a biochemical negative feedback loop, where A and $E_{i,o}$ are the controlled and controller species, respectively, we found that the reaction orders for the synthesis and removal reactions of $E_{i,o}$ (with respect to $E_{i,o}$) need to be identical. The resulting behaviors can show robust concentration homeostasis, however frequency homeostasis can also be observed when the considered systems are oscillatory.[17,22−29]

Before we describe the results of the different kinetic implementations of integral control, we give a brief overview of the kinetic requirements that lead to integral control. Figure 2b

Received: March 1, 2017
Revised: May 22, 2017
Published: June 2, 2017

DOI: 10.1021/acs.jpcb.7b01989
J. Phys. Chem. B 2017, 121, 6097−6107

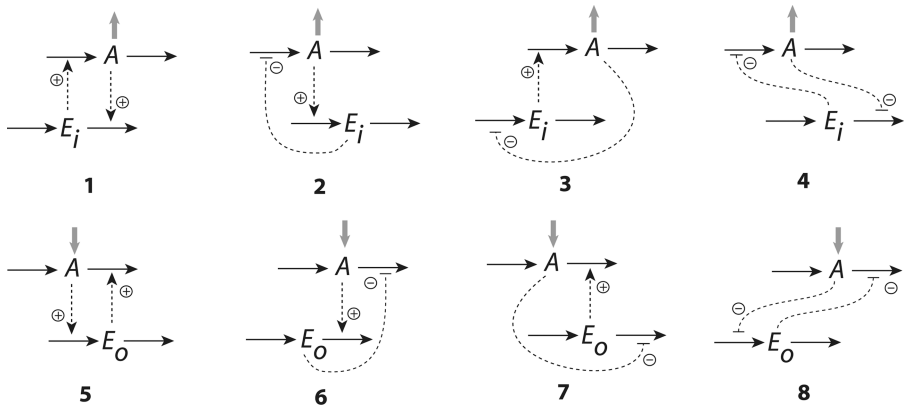

Figure 1. Eight basic negative feedback motifs. In motifs 1−4, the compensatory flux originating from E_i is an inflow to A (inflow controllers), whereas in motifs 5−8, the compensatory flux originating from E_o is an outflow from A (outflow controllers). Gray arrows indicate the perturbations that the motifs are able to oppose.

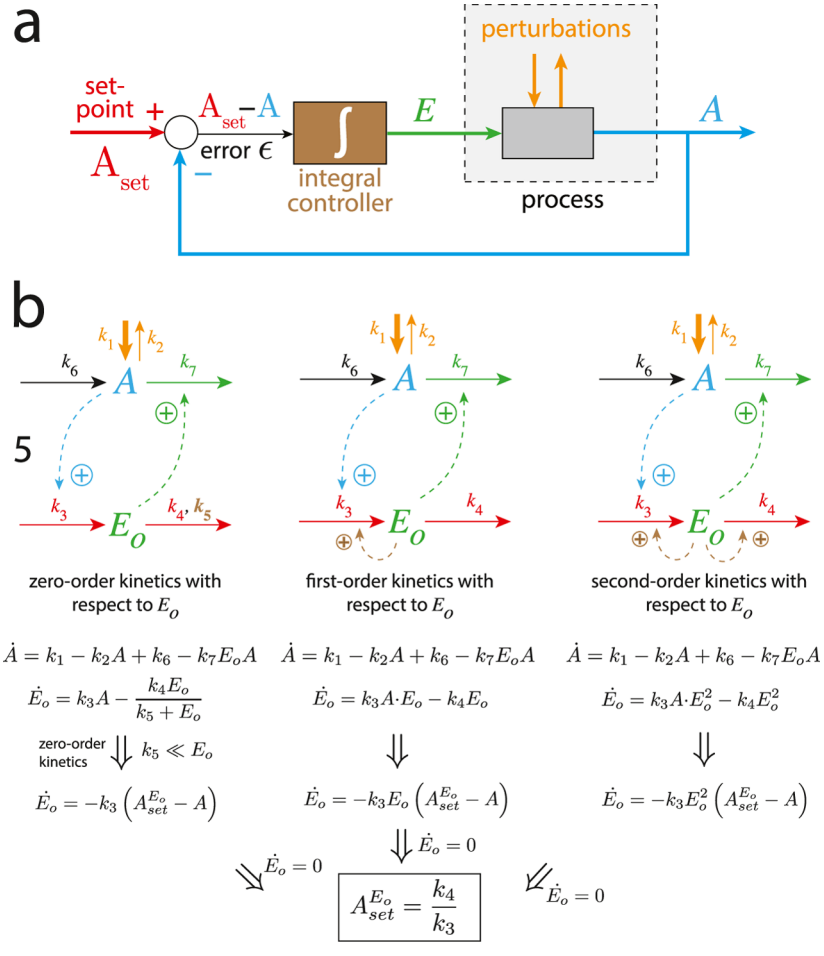

Figure 2. Implementation of integral control by three different kinetic mechanisms. (a) General control scheme. (b) Molecular representations of integral control using motif 5 as an example. By applying the steady state condition $\dot{k}_1/\dot{E}_o = 0$, the set-point of A for the three controllers is calculated to be $A_{set}^{E_o} = k_4/k_3$, independent of the values of k_1 and k_2, as long as the inflow perturbation k_1 dominates over outflow perturbation k_2.

shows the three types of integral control implementations that are considered in this study. The left scheme in Figure 2b shows how integral control can be incorporated by zero-order kinetics with respect to E_o. The two schemes in the middle and to the right of Figure 2b incorporate integral control by using first- and second-order autocatalysis and degradation with respect to E_o. The fluxes $j_1 = k_1$ and $j_2 = k_2 \cdot A$ describe environmental disturbances in A, whereas flux $j_6 = k_6$ is a system-internal synthesis of A. The flux $j_7 = k_7 \cdot A \cdot E_o$ is the compensatory outflow flux that neutralizes inflow perturbations. As an outflow controller can only compensate for inflow perturbations and an inflow controller can only compensate for outflow perturbations, a system that can handle both types of perturbations needs both inflow and outflow controllers to be present. This organization of inflow and outflow controllers appears to be the main reason why physiological controllers

DOI: 10.1021/acs.jpcb.7b01989
J. Phys. Chem. B 2017, 121, 6097−6107

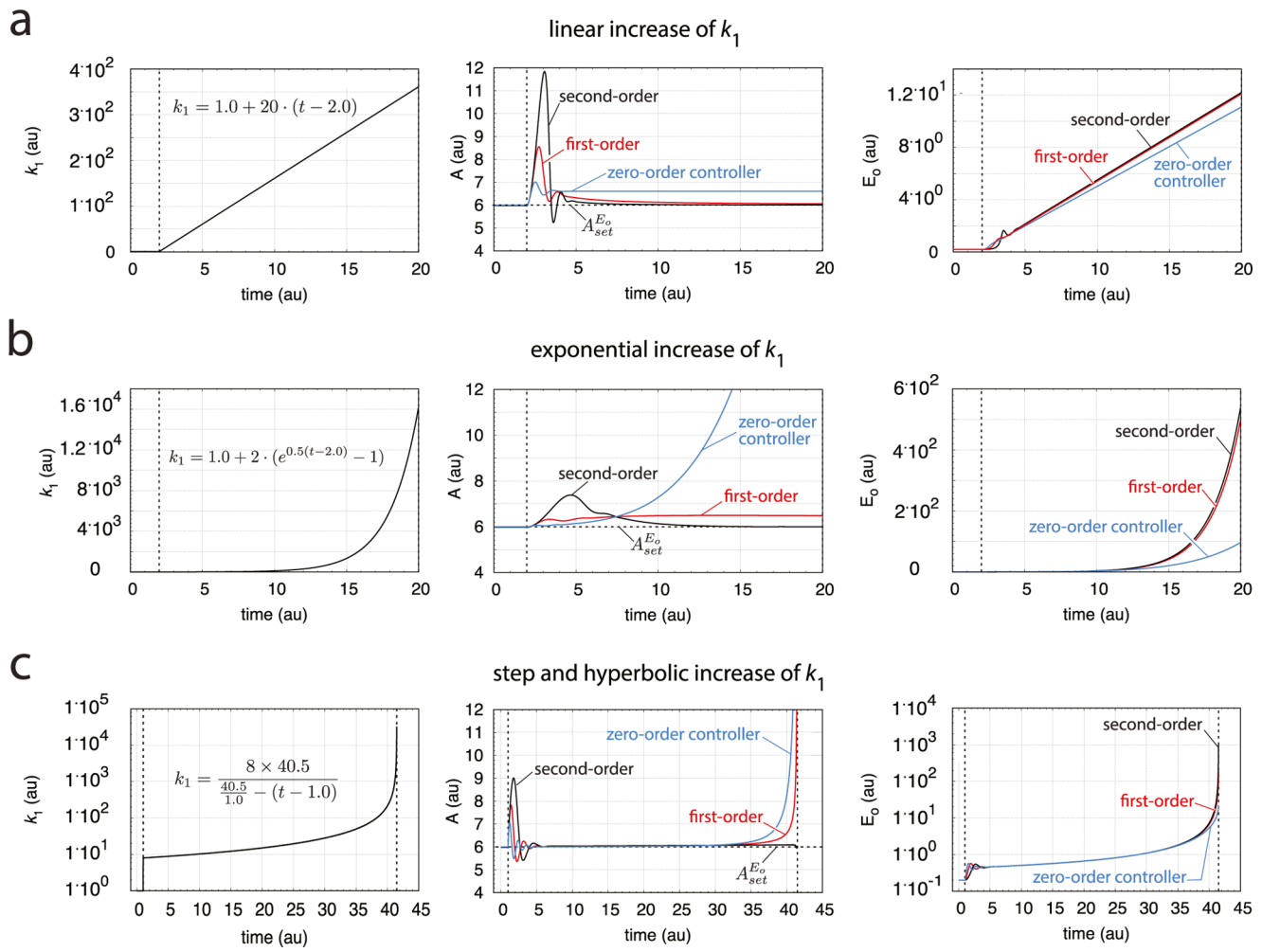

Figure 3. Performance of the three implementations of integral control (Figure 2b) for controller motif 5. Dashed vertical lines indicate phase borders. Dashed horizontal lines in middle panels indicate the set-point $A^{E_o}_{set}$ = 6.0. Left panels: (a) k_1 increases linearly using parameters $k_{1,p}$ = 1.0, α = 20.0, and t_p = 2.0 (eq 2). (b) k_1 Increases exponentially with parameters $k_{1,p}$ = 1.0, α = 2.0, β = 0.5, and t_p = 2.0 (eq 3). (c) k_1 has a step-wise increase at t_p = 1.0 and hyperbolic growth with parameters $k_{1,p}$ = 1.0, α = 40.5, and β = 8.0 (eq 4). Middle and right panels: blue curves show A and E_o values of the zero-order type of controller, whereas red and black curves show A and E_o values for the first- and second-order autocatalytic controllers, respectively. Rate constants: k_1 = 1.0 ($t < t_p$), k_2 = 0.0, k_3 = 1.0, k_4 = 6.0, $k_5 = 1 \times 10^{-4}$, $k_6 = k_7$ = 5.0, $k_{13} = k_{14} = 1 \times 10^{-3}$. Initial concentrations: A_0 = 6.0, $E_{o,0}$ = 0.2. The rate equations of the motif 5 controllers are given in SI2.

often come in antagonistic pairs.[30,31] As can be seen from Figure 2b, the rate equations for the three E_o's can be formulated as

$$\dot{E}_o = -k_3 \cdot E_o^{\gamma} \cdot (A^{E_o}_{set} - A) \quad (1)$$

where $A^{E_o}_{set} = k_4/k_3$ describes the perturbation-independent set-points for the three controllers with exponent γ equal to 0, 1, or 2. The color codes used in Figure 2 illustrate the functional relationships between the general flow scheme of Figure 2a and the molecular/reaction kinetic representations of Figure 2b. The red color indicates the rate constants k_3 and k_4 defining the set-point of the controller. The brown color indicates the parts that lead to integral control, that is, a low k_5 value in the zero-order type of controller and identical synthesis and degradation reaction orders with respect to E_o in the two autocatalytic controllers. Blue and green colors indicate the respective signaling reactions from A to E_o and from E_o to A, and the orange color indicates the perturbations.

Most of our earlier studies[17,22−29] on robust homeostasis were conducted by applying zero-order kinetics to achieve integral control and focused on properties in the face of different but constant perturbations. The goal of the present study is to compare how the different kinetic implementations of integral control influence overall controller performance. In biological systems, the perturbation strength by invasive agents often increases with time and may be relatively rapid, such as the exponential growth of pathogenic bacteria[32] or the hyperbolic/hypercyclic growth of viruses.[33] To meet attackers with minimal delay, the immune system, for example, produces and destroys lymphocytes all the time while maintaining a robust lymphoid homeostasis.[34] Because of such time-dependent aspects we, as a first approach, studied how different implementations of integral control will influence a controller's performance in maintaining homeostasis when growth and depletion perturbations show linear, exponential, or hyperbolic time dependencies.

METHODS

Controller performances are presented in complementary pairs of inflow/outflow controllers, that is, controller pairs 1 and 5, 2 and 6, 3 and 7, and 4 and 8 (Figure 1). The set-point values of A for the individual controllers were taken, rather arbitrarily, to

DOI: 10.1021/acs.jpcb.7b01989
J. Phys. Chem. B 2017, 121, 6097−6107

be either 3.0 or 6.0, dependent on the controller pairs. The set-point values (3.0 or 6.0) were chosen such that the combined complementary controllers do not show windup (see Supporting Information, ch. "Integral Windup in Combined Controllers" of ref 17).

Computations were performed by using the Fortran subroutine LSODE[35] in conjunction with Absoft's Pro Fortran compiler (www.absoft.com). The graphs were generated with gnuplot (www.gnuplot.info) and Adobe Illustrator (www.adobe.com). To make notations simpler, concentrations of compounds are denoted by compound names without square brackets. Rate parameters are presented as k_i's (i = 1, 2, 3, ...) irrespective of their kinetic nature, that is, whether they represent turnover numbers, Michaelis constants, or inhibition constants. A set of corresponding Matlab and Simulink calculations are provided in the Supporting Information (zip).

In the calculations, we consider two phases. In phase 1, starting at time $t = 0$, the concentration of A is kept constant either at set-point $A_{\text{set}}^{E_i}$ or at $A_{\text{set}}^{E_o}$ (dependent on whether the controller is of the inflow or outflow type) using constant k_1/k_2 values. At time $t = t_p$, phase 2 starts and the values of k_1 or k_2 are changed using the following time dependencies.

(i) the A-perturbation is a linear function of time t

$$k_{1/2} = k_{1/2,p} + \alpha\cdot(t - t_p);\ \ t \geq t_p \tag{2}$$

$k_{1/2}$ denotes either k_1 or k_2; $k_{1/2,p}$ is the k_1 or k_2 value at time t_p, and α is a positive constant.

(ii) the perturbation has an exponential time dependency

$$k_{1/2} = k_{1/2,p} + \alpha(e^{\beta\cdot(t-t_p)} - 1);\ \ t \geq t_p \tag{3}$$

(iii) the perturbation has a hyperbolic time dependency

$$k_{1/2} = \frac{\alpha\cdot\beta}{\frac{\alpha}{k_{1/2,p}} - (t - t_p)};\ \ t \geq t_p \tag{4}$$

Note that $k_{1/2}$ goes to infinity when t reaches $(\alpha/k_{1/2,p}) + t_p$. A value of $\beta > 1$ in eq 4 allows for an additional step-wise change of k_1 or k_2 at $t = t_p$.

RESULTS AND DISCUSSION

In the following discussion, we present four of the eight controller motifs and show how the three implementations of integral control (Figure 2b) can manage to maintain homeostasis against linear, exponential, and hyperbolic changes in k_1/k_2. The controllers described in the main part of this article are inflow controllers 2 and 3 and outflow controllers 5 and 8. The other controllers, respectively, 6 and 7, and 1 and 4 show similar/analogous behaviors to those covered in the main article. They are described in the Supporting Information (see below).

Responsiveness of Autocatalytic Controllers. A problem the autocatalytic implementation of integral control faces is that low concentrations of the controller variables E_o or E_i may lead to unresponsive or slow responding controllers. The reason for this can be explained by looking at the equation for the change in $E_{i,o}$, for example, eq 1 for outflow controller 5. The first- and second-order autocatalytic controllers (γ = 1, 2) have a reaction rate in $E_{i,o}$ that is dependent upon its own concentration and leads to self-amplifying positive feedback. However, when $E_{i,o}$ is zero, none of the autocatalytic controllers are able to start up. Thus, care has to be taken to avoid situations where $E_{i,o}$ is driven toward too low values. An example of how this may occur is given in the Supporting Information (SI1). To prevent situations with too low $E_{i,o}$ values, in the following calculations we kept $E_{i,o}$ at basal levels by including small synthesis and degradation rates with the respective rate constants k_{11} and k_{12} for the autocatalytic inflow controllers E_i, and k_{13} and k_{14} for the autocatalytic outflow controllers E_o. The rate constants are in the order of $10^{-3}/10^{-2}$ and have no practical influence on the set-points for the autocatalytic controllers.

Controller Motifs with Activating Signaling. *Motifs 5 and 1.* In motif 5 (and complementary motif 1), the signaling mechanisms between A and E are entirely based on activation. Figure 3 gives an overview of how the different kinetic implementations of integral control behave for motif 5. Typically, the zero-order implementation can keep A only at its set-point for step-wise perturbations in A. If the perturbation k_1 increases linearly, the A value of the controller shows a systematic but constant offset from $A_{\text{set}}^{E_o}$ (Figure 3a, middle panel, blue curve). The steady state value of A (A_{ss}) for an ideal zero-order controller (when $k_5 \to 0$) can be calculated by assuming that $\dot{A}$ and $\ddot{A}$ vanish. A_{ss} in this case is given by (SI2)

$$A_{ss} = \frac{1}{2}A_{\text{set}}^{E_o} + \sqrt{\left(\frac{1}{2}A_{\text{set}}^{E_o}\right)^2 + \frac{\dot{k}_1}{k_3 k_7}} \tag{5}$$

with $\dot{k}_1/(k_3k_7)$ contributing to the offset. Thus, with increasing but constant $\dot{k}_1$ the offset for the zero-order type of controller increases, but can be reduced by increasing the values of k_3 and/or k_7. As indicated by eq 5 and Figure 3b,c (middle panel, blue curves), the zero-order type of controller breaks down when the rate law for k_1 exceeds linear time kinetics.

Considering the first-order autocatalytic implementation of integral control into motif 5, the controller is able to establish a steady state for power-law and exponential perturbations in A. However, for exponential perturbations, the controller shows a constant offset above $A_{\text{set}}^{E_o} = 6.0$ (Figure 3b, middle panel, red curve). The controller is not able to counteract hyperbolic perturbations in A. The second-order autocatalytic implementation of integral control shows the best results with relatively small offsets when perturbations become hyperbolic (Figure 3c, middle panel, black curve).

The offset for the two autocatalytic controllers can be calculated from the stationary solutions in A, which take the following form (SI2)

$$A_{ss} = \frac{1}{2}A_{\text{set}}^{E_o} + \sqrt{\left(\frac{1}{2}A_{\text{set}}^{E_o}\right)^2 + \frac{\dot{k}_1}{E_o^n\cdot k_3\cdot k_7}} \tag{6}$$

where n is either 1 or 2, dependent on whether autocatalysis in E_o is first- or second-order, respectively. Equation 6 also shows that for the autocatalytic controllers, $A_{ss} \to A_{\text{set}}^{E_o}$ as long as E_o^n increases faster than $\dot{k}_1$. A comparison between the numerical A-values and the stationary values A_{ss} is also given in SI2.

SI3 shows corresponding results for the complementary motif 1.

Controller Motifs with Activating and Inhibiting Signaling. This class contains four negative feedback arrangements (Figure 1). In two of them, motifs 2 and 6, A activates, respectively, the synthesis of E_i or the removal of E_o, and the $E_{i,o}$'s either inhibit the compensatory influx to A (motif 2) or the compensatory outflux from A (motif 6). In motifs 3 and 7, the A/E inhibitions/activations are reversed, that is, A inhibits

DOI: 10.1021/acs.jpcb.7b01989
J. Phys. Chem. B 2017, 121, 6097−6107

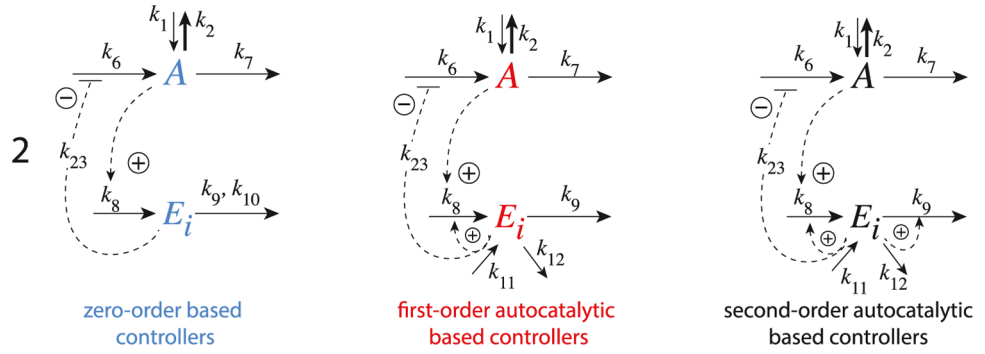

Figure 4. Kinetic implementations of integral control for motif 2. See SI4 for rate equations, initial conditions, and derivations of the stationary solutions A_{ss}.

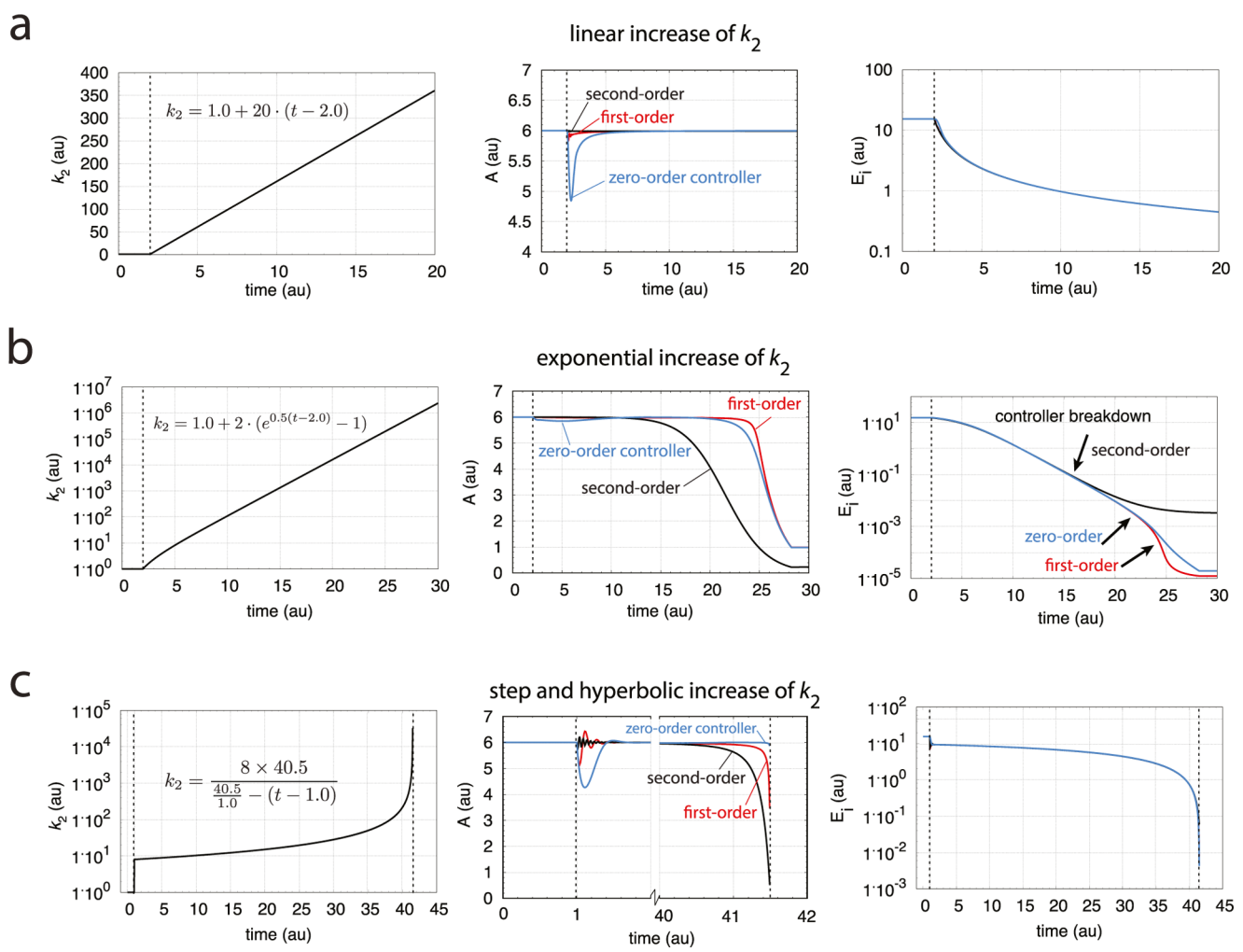

Figure 5. Performance of the three implementations of integral control in motif 2. During the first phase from $t = 0$ until the dashed line at $t = t_p = 2.0$, we have $k_1 = k_2 = 1.0$. During the second phase, k_1 remains unchanged and k_2 increases as indicated in the left panels. Middle panels show the changes in A and adaptation of A to the controllers' set-points at $A_{set}^{E_i} = 6.0$. Color coding is as in Figure 3. As indicated in the middle and right panels of (b) and (c), the controllers are no longer able to maintain homeostasis as E_i levels drop too low. SI4 describes the rate equations, rate constant values, and initial concentrations.

the synthesis of E_i or the removal of E_o, respectively, and the $E_{i,o}$'s activate either the compensatory influx (motif 3) or the compensatory outflux (motif 7).

Motifs 2 and 6. The negative feedback structure of motif 2 is closely related to the Goodwin equations,[36−38] which have been used in many variations as a model for different types of biological oscillators.[39]

Figure 4 shows the three implementations of integral control in motif 2. As this is an inflow controller, we tested the controller against changes in k_2. To compensate for the outflow perturbations induced by k_2, the E_i levels for this feedback type need to decrease to raise the compensatory flux $j_6 = k_6k_{23}/(k_{23} + E_i)$ to keep A at its set-point. For continuously increasing k_2 values, the motif 2 controllers will eventually break down

DOI: 10.1021/acs.jpcb.7b01989
J. Phys. Chem. B 2017, 121, 6097−6107

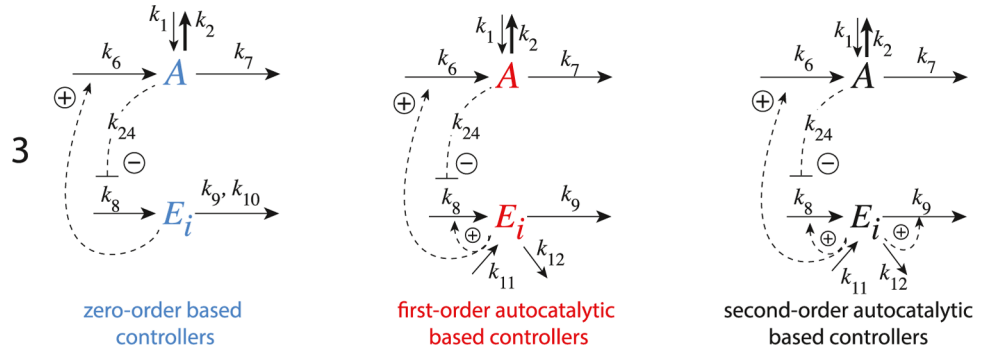

Figure 6. Kinetic implementations of integral control for motif 3. See SI6 for rate equations, initial conditions, and derivations of the stationary solutions A_{ss}.

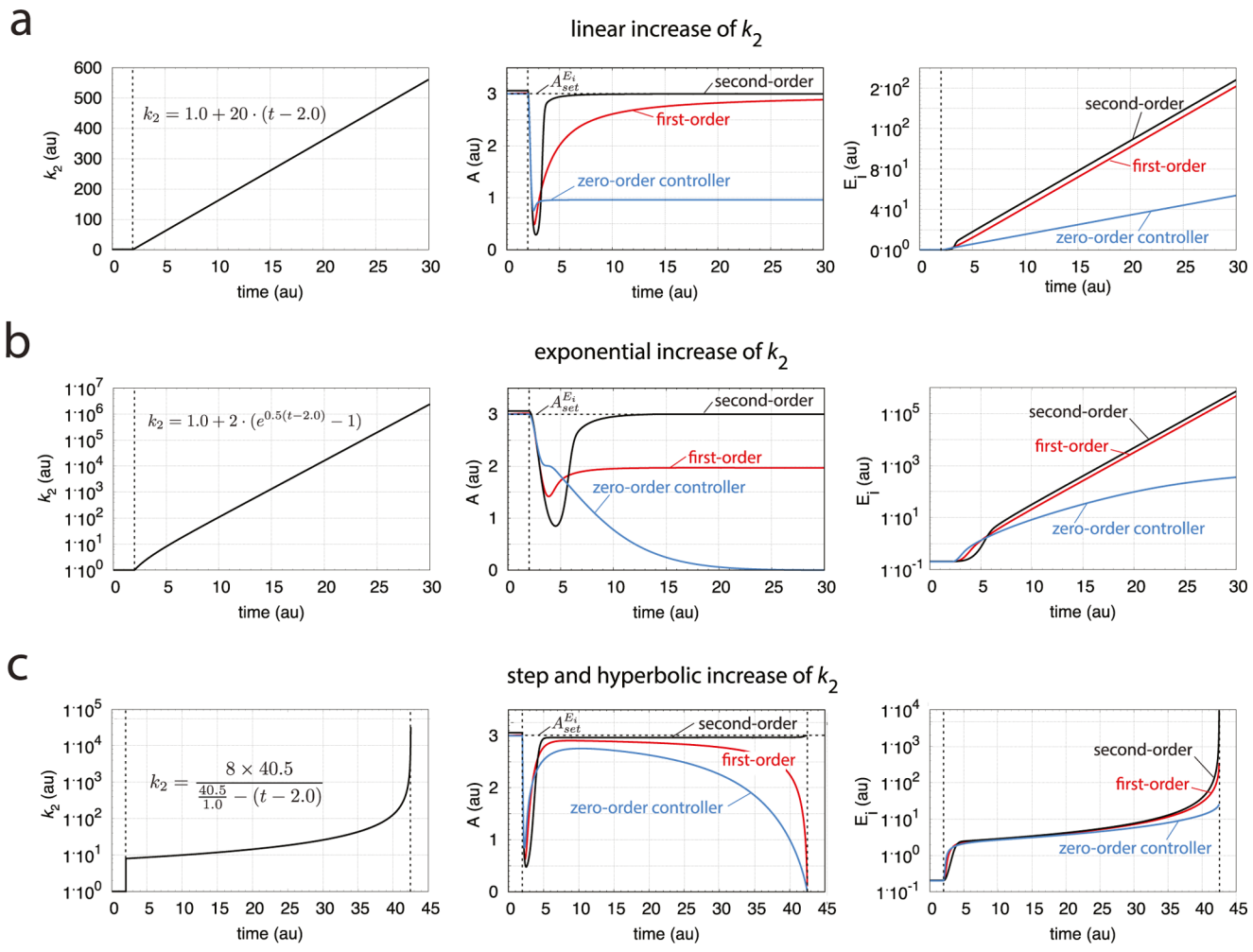

Figure 7. Performance of the three implementations of integral control in controller motif 3 (Figure 6). During the first phase from $t = 0$ to $t = t_p = 2.0$, we have $k_1 = k_2 = 1.0$. During phase 2 ($t > t_p$), $k_1 = 1.0$ and k_2 increases as indicated in the left panels. Middle panels show the changes in A and the controllers' ability to maintain the set-point $A_{set}^{E_i} = 3.0$. Color coding is as in Figure 3. SI6 describes the rate equations, rate constant values, and initial concentrations.

because when the E_i level gets too low, the controller will no longer be able to maintain the function of the negative feedback loop.

Figure 5 shows how the different controller implementations behave toward linear, exponential, and hyperbolic increases in k_2. A striking difference with the controllers based on motif 5 (and 1) is the apparent lack of an offset in A. The stationary solutions of the three controllers are (SI4)

$$A_{ss} = A_{set}^{E_i}\left(\frac{\gamma_n}{1+\gamma_n}\right) \tag{7}$$

where

$$A_{set}^{E_i} = \frac{k_9}{k_8} \tag{8}$$

is the set-point, and

DOI: 10.1021/acs.jpcb.7b01989
J. Phys. Chem. B 2017, 121, 6097−6107

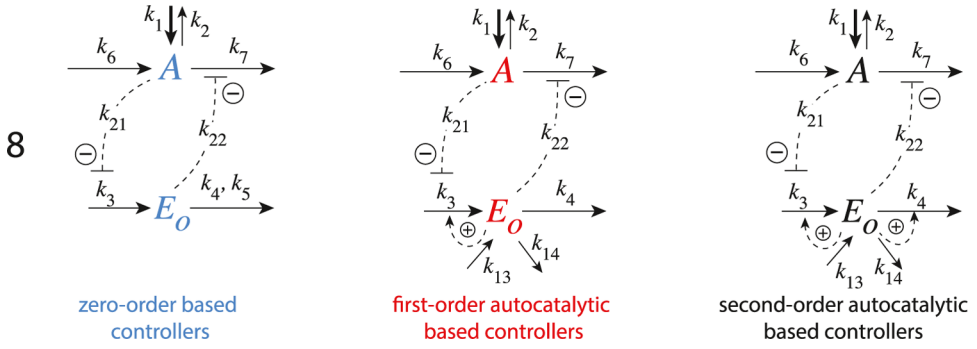

Figure 8. Kinetic implementations of integral control for motif 8. Rate equations and initial conditions are described in SI8.

$$\gamma_n = \frac{k_6 k_8 k_{23} E_i^n}{\dot{k}_2 (k_{23} + E_i)^2} \tag{9}$$

relates to the offset contribution for the zero-order, first-order, and second-order controllers with n = 0, 1, 2, respectively. High γ_n values indicate a controller that is able to keep A close to its set-point (Figure 4) such that $\gamma_n/(1 + \gamma_n) \approx 1$ (see also SI4).

Interestingly, the zero-order implementation of integral control performs better than the two autocatalytic controllers, that is, when A is rapidly removed in a hyperbolic fashion (Figure 5c, middle panel), while under these conditions, the second-order autocatalytic controller performs the poorest. The reason for the better performance of the zero-order arrangement lies in the nonlinear dynamics of the inhibition term, which allows E_i to decrease as rapidly as the perturbation occurs. With a rapidly increasing k_2, the perturbation-induced decrease of E_i in the zero-order type of controller is sufficiently quick to maintain homeostasis even for very high $\dot{k}_2$ values. For the autocatalytic controllers, however, the E_i decrease is slightly slower due to the autocatalytic production terms in E_i, which oppose an effective decrease in E_i (SI4).

For the complementary outflow controllers based on motif 6, analogous behaviors as seen for motif 2 are observed, that is, the zero-order controller performs considerable better than the controllers based on autocatalysis. SI5 shows the results.

Motifs 3 and 7. Because of its feedback structure, motif 3-based controllers compensate outflow perturbations by an increase in E_i. The different implementations of integral control in motif 3 are indicated in Figure 6, and Figure 7 shows an overview of the performance of the different implementations. In contrast to those of motif 2, but like those of motif 5, the motif 3-based controllers show offsets from $A_{set}^{E_i}$ (now negative) when the zero-order, first-order, or second-order controllers encounter, respectively, a linear, exponential, or hyperbolic increase in k_2 (Figure 7, middle panels). The offsets can be calculated by the stationary solutions A_{ss}. For the zero-order type of controller, A_{ss} is given by

$$A_{ss} = -\left(\frac{\gamma_0 + k_{24}}{2}\right) + \sqrt{\left(\frac{\gamma_0 + k_{24}}{2}\right)^2 + \gamma_0 A_{set}^{E_i}} \tag{10}$$

where in this case

$$\gamma_0 = \frac{k_6 k_9}{\dot{k}_2} \tag{11}$$

and

$$A_{set}^{E_i} = k_{24}\left(\frac{k_8}{k_9} - 1\right) \tag{12}$$

When $\dot{k}_2 = 0$, $A_{ss} = A_{set}^{E_i}$ (see SI6, page S37). Equation 10 is in excellent agreement with the numerical data (Figure S2, SI6). For the first- and second-order autocatalytic controllers, A_{ss} is analogous to eq 10, where γ_0 is replaced by γ_n

$$\gamma_n = \frac{k_6 k_9 E_i^n}{\dot{k}_2} \tag{13}$$

where n is 1 and 2 for the first-order and second-order autocatalytic controllers, respectively. The derivations of eqs 10−13 and a comparison between A_{ss} and the numerical A-values for the controllers are described in SI6. Although the second-order autocatalytic controller performs best, its A steady state shows a certain but minor offset below $A_{set}^{E_i} = 3.0$ when the outflow perturbation is hyperbolic (Figure S4 in SI6).

SI7 shows the corresponding results for the three integral control implementations for motif 7.

Controller Motifs with Inhibiting Signaling. *Motifs 8 and 4.* Finally, we turn to motif 8, which contains only inhibitory signaling. The motif 8-based controllers are outflow controllers and maintain homeostasis against inflow perturbations by an increase in the outflow compensatory flux. This is achieved by decreasing E_i. The implementations of integral control for controller 8 are shown in Figure 8. Rate equations, rate constant values, and initial conditions are stated in SI8.

The controllers' responses toward a linear increase in k_1 with time (Figure 8) show that the zero-order and the first-order autocatalytic controller can maintain homeostasis after a brief excursion. The second-order autocatalytic controller, on the other hand, is not able to keep homeostasis and shows increasing A-levels drifting away from the set-point $A_{set}^{E_o} = 6.0$.

The stationary solutions A_{ss} for the zero-order and autocatalytic controllers are as follows (see SI8 for derivation)

$$A_{ss} = \frac{\gamma_0}{2} + \frac{1}{2}A_{set}^{E_o} + \sqrt{\left(\frac{A_{set}^{E_o}}{2}\right)^2 + \frac{1}{2}A_{set}^{E_o}\gamma_0 + \left(\frac{\gamma_0}{2}\right)^2 + k_{21}\gamma_0} \tag{14}$$

with

$$\gamma_0 = \frac{\dot{k}_1 (k_{22} + E_o)^2}{k_4 k_7 k_{22}} \tag{15}$$

For the autocatalytic controllers, γ_0 is replaced in eq 14 by

DOI: 10.1021/acs.jpcb.7b01989
J. Phys. Chem. B 2017, 121, 6097−6107

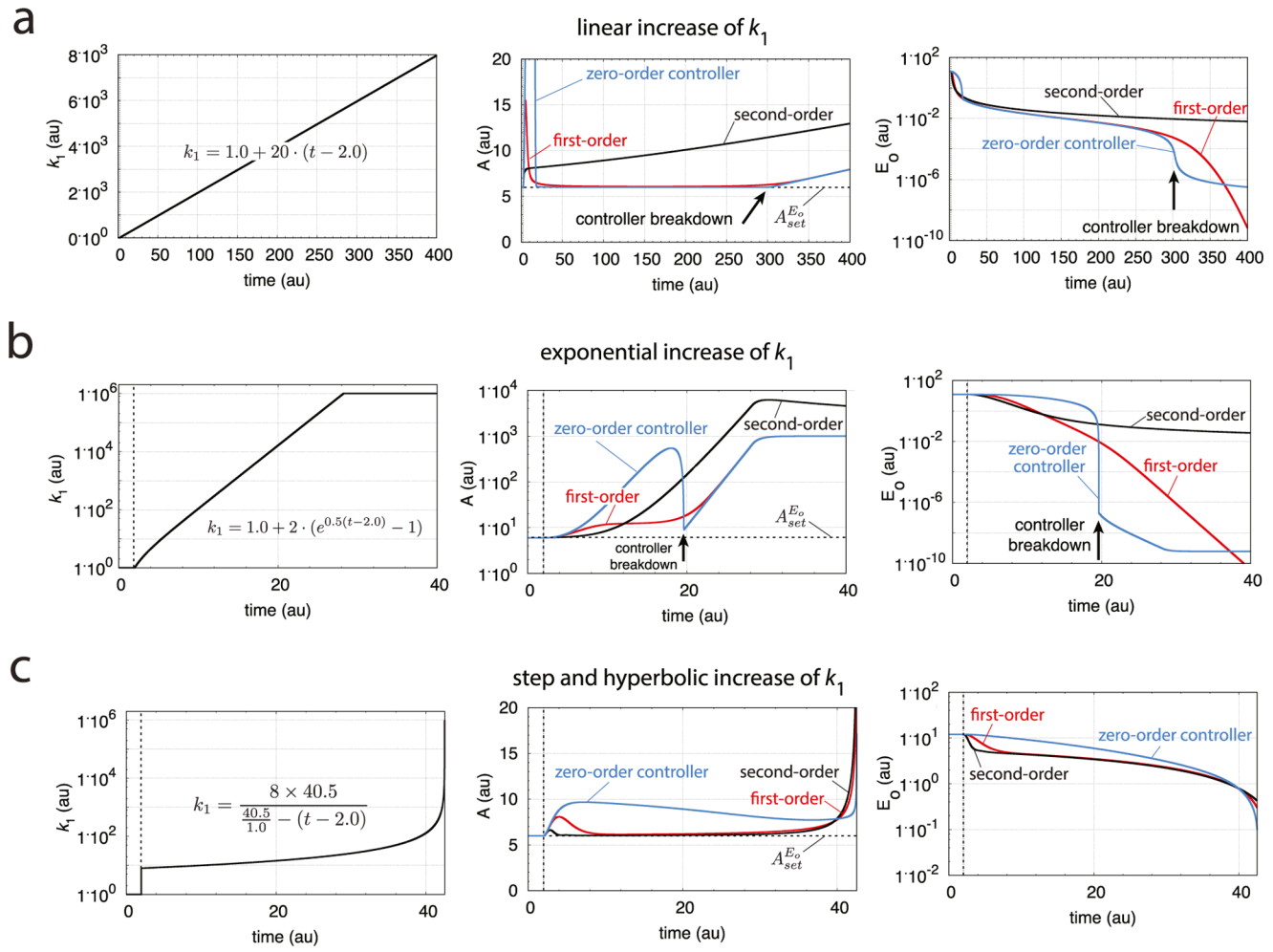

Figure 9. Performance of the three implementations of integral control in controller motif 8 (Figure 8). See SI8 for rate equations, rate constant values, and initial concentrations.

Table 1. Overview of the Influence of Feedback Structure and the Type of Integral Control Implementations on the Controllers' Homeostatic Performances with respect to Linear, Exponential, and Hyperbolic Time Dependencies in k_1/k_2

		type of integral control implementation		
controller motifs	time dependence of k_1/k_2 Increase	zero-order	first-order	second-order
1, 5 (Figure 3, SI2, SI3)	linear	constant A-offset, dependent on $\dot{k}_1/\dot{k}_2$	functional controller	functional controller
	exponential	controller breakdown	constant A-offset, dependent on $\dot{k}_1/\dot{k}_2$	functional controller
	hyperbolic	controller breakdown	controller breakdown	constant or small increasing A-offset
2, 6 (Figure 5, SI4, SI5)	linear	functional controller, breakdown at high k_1/k_2 values	functional controller, breakdown at high k_1/k_2 values	constant or increasing A-offset
	exponential	functional controller, breakdown at high k_1/k_2 values	breakdown at high k_1/k_2 values	controller breakdown
	hyperbolic	breakdown at high k_1/k_2 values	breakdown at high k_1/k_2 values	controller breakdown
3, 7 (Figure 7, SI6, SI7)	linear	constant A-offset, dependent on $\dot{k}_1/\dot{k}_2$	functional controller	functional controller
	exponential	controller breakdown	constant A-offset, dependent on $\dot{k}_1/\dot{k}_2$	functional controller
	hyperbolic	controller breakdown	controller breakdown	constant or small increasing A-offset
4, 8 (Figure 9, SI8, SI9)	linear	functional controller, breakdown at high k_1/k_2 values	functional controller, breakdown at high k_1/k_2 values	controller breakdown
	exponential	breakdown at high k_1/k_2 values	controller breakdown	controller breakdown
	hyperbolic	controller breakdown	controller breakdown	controller breakdown

$$\gamma_n = \frac{\dot{k}_1(k_{22} + E_o)^2}{k_4 k_7 k_{22} E_o^n} \quad (16)$$

with $n = 1$ for the first-order and $n = 2$ for the second-order controller. For the linear increase of k_1, the γ_0 and γ_1 values for the zero- and first-order type of controllers are, at $t = 100.0$,

DOI: 10.1021/acs.jpcb.7b01989
J. Phys. Chem. B 2017, 121, 6097−6107

respectively, 1.9×10^{-3} and 9.1×10^{-2}. These values decrease with decreasing E_o and show that the two controllers can keep homeostasis at $A_{set}^{E_o}$ with a relatively high accuracy. However, with increasing time, E_o becomes too low and the negative feedback loop cannot be operated any longer: the controllers break down. This is seen in Figure 9a, in the middle and right panels, where the zero-order and first-order controllers' breakdown occurs at about 300 time units. The A-levels of the two controllers then rise in parallel with the A-level of the already nonfunctional second-order controller. When k_1 increases exponentially (Figure 9b), none of the controllers are able to defend their set-points. Although the zero-order type of controller shows a temporary decrease toward $A_{set}^{E_o}$, breakdown occurs at about 20 time units and A-levels increase exponentially as for the other controllers. When k_1 increases hyperbolically, the autocatalytic controllers are able to move A to their set-points during the slow increasing phase of k_1, but controller breakdown occurs when k_1 comes close to singularity where $\dot{k}_1$ grows at an extremely rapid rate.

SI9 shows the results for the complementary motif 4.

Comparison of Controllers. Table 1 gives a qualitative overview of the controllers' performances with respect to the perturbation kinetics k_1 and k_2 and the types of integral control implementation. A controller is considered functional when the A-offset between A and the controller's set-point, $|A - A_{set}^{E_{i/o}}|$, decreases with time, as judged from the calculations and the derived γ_n values. When a controller's intrinsic compensation kinetics match the kinetics of the perturbation, as indicated by a constant γ_n value, then constant A-offsets are observed. Controller breakdown occurs when the A-offset increases monotonically with time.

For controller motifs 1, 3, 5, and 7, where increasing k_1/k_2 values are compensated by an increased activation of $E_{i/o}$, the functionality of these controllers relies on a sufficient production rate of $E_{i/o}$. In our present formulation of these controllers, we allowed an ideal performance in the sense that controllers have an infinite capacity to generate $E_{i/o}$. When k_1 or k_2 is kept constant after a time-dependent perturbation, the A-values of these controllers will always return to their set-points (although this may take some time) even when the controllers had a breakdown during the preceding time-dependent k_1 or k_2 perturbation. However, controllers based on motifs 2, 4, 6, and 8 require decreased $E_{i/o}$ values to increase their compensatory fluxes. These controllers face the problem that a time-dependent increase in k_1/k_2 will eventually drive the $E_{i/o}$ values to such low levels that the compensatory fluxes become saturated and the controllers break down. After breakdown, the controllers are not able to return to their set-points once $\dot{k}_1$ or $\dot{k}_2$ is kept constant; they are trapped in their breakdown steady states. To illustrate this point, we take the motif 8-based controllers as an example. The rate equation of A for this motif is (SI8)

$$\dot{A} = k_1 + k_6 - k_2 A - \frac{k_7 k_{22} A}{k_{22} + E_o} \tag{17}$$

Assuming that the three controller types based on this motif can keep their steady states in A at the set-point $A_{set}^{E_o}$, we can calculate the steady state concentration of E_o as a function of different but constant k_1 values

$$E_{o,ss} = \frac{k_7 k_{22} A_{set}^{E_o}}{k_1 + k_6 - k_2 A_{set}^{E_o}} - k_{22} \tag{18}$$

Equation 18 shows that as k_1 increases, $E_{o,ss}$ becomes zero or even negative. Negative $E_{o,ss}$ values are unphysical, which indicates that A_{ss} at such high k_1 values has to deviate from $A_{set}^{E_o}$ and that the controllers cannot keep their A-values at the set-point. Thus, if a time-dependent k_1 drives the controllers eventually into breakdown and then $\dot{k}_1$ is kept constant, the remaining steady state is given by eq 18, with $A_{set}^{E_o}$ replaced by A_{ss}, where A_{ss} is larger than $A_{set}^{E_o}$. As E_o is driven to very low values and the derepression mechanism becomes saturated ($E_o \ll k_{22}$), an approximate value of A_{ss} can be estimated from eq 17, that is

$$A_{ss} \approx \frac{k_1 + k_6}{k_2 + k_7} \text{ (high } k_1\text{)} \tag{19}$$

This shows that the controllers based on derepression of the compensatory flux have a finite operational lifetime once exposed to perturbations that grow in time. With increasing constant or accelerating $\dot{k}_1$ or $\dot{k}_2$ values, the operational lifetime of these controllers decreases. For the motif 1, 3, 5, and 7-based controllers, constant A-offsets occur when the internal controller and perturbation kinetics are of the same order (e.g., a first-order controller acting on an exponentially increasing perturbation). In these cases, the $\dot{k}_1$ or $\dot{k}_2$ values are part of the parameter set that determines the size of the offset, as indicated by the expressions for the derived γ_n values (see SI6 and SI7). When the controller kinetics are superior to the kinetics of the perturbation (e.g., when a first-order controller is acting on a linearly increasing perturbation), homeostasis is always guaranteed as long as sufficient $E_{i/o}$ can be produced (however, see discussion below when the $E_{i/o}$'s are considered to become limiting).

Taking our earlier observations for the zero-order implementation of integral control that all eight controller motifs can successfully defend their homeostatic set-points with little difference for step-wise perturbations (Figure 2 in ref 17), it is interesting to note the large differences between the controllers when they become exposed to perturbations with different time-changing kinetics.

These differences in the controllers' behaviors come both from the different kinetic implementations of integral control and from the type of signaling kinetics, which can be either of an activating or inhibiting type. An explanation of the observations can be found in the *Internal Model Principle*,[40−42] which states that if a controller adapts to an environmental perturbation, then the controller needs to have the capability to generate that type of perturbation internally. This is, for example, seen in Figure 3c for outflow controller 5, where the second-order autocatalytic implementation of integral control adapts to the hyperbolic increase in A by increasing E_o hyperbolically (although with a steady state slightly off $A_{set}^{E_o}$). On the other hand, neither the zero-order nor the first-order controllers have the kinetic capability to generate E_o hyperbolically and are therefore not able to compensate for a hyperbolically increasing inflow of A.

The behavior of the controllers based on motif 2 (Figure 4) can be understood in a similar manner: a rapid decrease in A leads to a decrease in E_i, which then derepresses the compensatory flux j_6. As indicated by the stationary solutions (SI4), the remarkable ability of this feedback arrangement is that all three integral control implementations can show adaptation to their set-points practically without an offset (Figure 5). The reason why the second-order autocatalytic

DOI: 10.1021/acs.jpcb.7b01989
J. Phys. Chem. B 2017, 121, 6097−6107

controller (Figure 5b,c, middle panels) performs more poorly than the zero-order type of controller is because the autocatalytic production part of E_i hinders an efficient hyperbolic decrease in E_i (Figure 5b, right panel).

In controller motif 3, offsets from the set-point are observed for all three controllers whenever the rate law of the increasing k_2 is the same or is more rapid than the rate-law generating E_i. The second-order autocatalytic controller performs best, followed by the first- and zero-order controllers.

The controllers based on motif 8 performed poorly: the second-order autocatalytic controller fails when k_1 increases linearly, whereas the zero- and first-order controllers can maintain homeostasis until E_o becomes too low and the negative feedback loops are no longer operational (controller breakdown, Figure 9). When k_1 increases exponentially, the zero-order type of controller makes an attempt to move A to its set-point, but controller breakdown occurs when E_o rapidly drops to low values (Figure 9b). During the initial phase of the hyperbolic perturbation, k_1 increases slowly such that the autocatalytic controllers can move A to their set-points (Figure 9c, middle panel), but as k_1 increases, its growth rate homeostasis is lost for all controllers.

The results can be summarized as follows: all controllers are able to maintain homeostasis for moderate step-wise changes in k_1 or k_2,[17] or when the perturbing k_1/k_2 changes (relative to the controllers' responsiveness) are slow (Figures 3c, 5c, and 9c, middle panels). To avoid potential failures in the start-up of the autocatalytic controllers at low E_i or E_o concentrations, these controllers need to have slightly elevated resting levels in E_i and E_o. All controllers where the signaling from $E_{i/o}$ to A is of the activating type (and first-order with respect to E_i or E_o) show a constant offset from the set-point whenever the rate law of the k_1/k_2 increase is the same as that for the compensatory flux. The usage of an activating signaling from A to $E_{i/o}$ and an inhibitory signaling from $E_{i/o}$ to A combined with zero-order implementation of integral control shows the best results with respect to avoiding offsets and maintaining homeostasis with different step-wise and time-dependent perturbations.

Although controller motifs 2 and 6 with a zero-order implementation of integral control show the best performance, the only drawback, it appears, is that these controllers eventually break down when their $E_{i/o}$ values become too low. However, a restricted range of $E_{i/o}$ does not only apply to controller motifs with inhibitory signaling but also to those where the signaling is entirely of the activating type (motifs 1 and 5). The reason for this is that a cell or organism will eventually reach a limit of saturation or capacity to make more $E_{i/o}$. Thus, all controllers, irrespective of how well they perform, when exposed to a time-dependent perturbation will eventually show breakdown when $E_{i/o}$ reaches either the upper or lower bounds of their operational range. Interestingly, this type of controller breakdown is reminiscent of Selye's *General Adaptation Syndrome (GAS)*.[5,43] When continuously exposed to stress (cold, drugs, or forced work), Selye observed that animals show a certain reaction pattern: during the first phase, the so-called "alarm reaction", animals react to the stressor and prepare for physical activity; during the second phase, termed the "stage of resistance", animals have adapted to the stressor and are in a stage of apparent well-being similar to the unstressed animals; in the final phase, the "stage of exhaustion", the resistance collapses and animals die. Selye interpreted the surprising collapse as a loss of "adaptation energy".[4,5,44] Certainly, organisms are considerably more complex in their physiological regulations than the single negative feedback loops considered here; still, we are intrigued by this puzzling analogy.

CONCLUSIONS

This is the first study where different implementations of integral control were used to test homeostatic capabilities on a set of basic controller motifs when perturbations change linearly, exponentially, and hyperbolically with time. For controllers where the compensatory flux is activated by controller variable $E_{i/o}$, the controllers can cope with rapidly growing or depleting perturbations whenever sufficient $E_{i/o}$ is supplied and the integral control implementation is at least of the same kinetic order as the perturbation (motifs 1, 3, 5, and 7). Controllers where the compensatory flux is based on inhibition already have an inherent hyperbolic rate law in their compensatory fluxes (internal model principle) and can cope with the applied time perturbations in k_1 and k_2 (motifs 2, 4, 6, and 8). For these controllers, the zero-order implementation of integral control provides the best control design, because higher-order implementation of integral control hinders an effective decrease in $E_{i/o}$. Aspects that will be investigated in future work are how the kinetics of the signal transduction chains influence controller performance and controller accuracy.

ASSOCIATED CONTENT

Supporting Information

The Supporting Information is available free of charge on the ACS Publications website at DOI: 10.1021/acs.jpcb.7b01989.

Responsiveness of autocatalytic controllers in combined inflow and outflow controllers 1 and 5; comparing stationary and numerical solutions of A with the different implementations of integral control for motif 5; comparing controller performances, and stationary and numerical solutions of A using the different implementations of integral control for motif 1; comparing stationary and numerical solutions of A with the different implementations of integral control for motif 2; comparing controller performances, and stationary and numerical solutions of A using the different implementations of integral control for motif 6; comparing stationary and numerical solutions of A with the different implementations of integral control for motif 3; comparing controller performances, and stationary and numerical solutions of A using the different implementations of integral control for motif 7; comparing stationary and numerical solutions of A with the different implementations of integral control for motif 8; comparing controller performances, and stationary and numerical solutions of *A* using the different implementations of integral control for motif 4 (SI1−SI9) (PDF)

Matlab and Simulink files showing the behaviors of different implementations of integral control for motif 5 (Figure 3), motif 2 (Figure 5), motif 3 (Figure 7), and motif 8 (Figure 9) (ZIP)

AUTHOR INFORMATION

Corresponding Author

*E-mail: peter.ruoff@uis.no.

ORCID

Peter Ruoff: 0000-0003-4430-0382

DOI: 10.1021/acs.jpcb.7b01989
J. Phys. Chem. B 2017, 121, 6097−6107

Notes

The authors declare no competing financial interest.

■ ACKNOWLEDGMENTS

The paper is dedicated to J.C. Dunlap on the occasion of his 65th birthday. The research was financed in part by a strategic Ph.D. Fund from the University of Stavanger to GF.

■ REFERENCES

(1) Cannon, W. Organization for Physiological Homeostasis. *Physiol. Rev.* **1929**, *9*, 399−431.
(2) Cannon, W. B. *The Wisdom of the Body*; Norton: New York, 1939.
(3) Langley, L. L., Ed.; *Homeostasis. Origins of the Concept*; Dowden, Hutchinson & Ross, Inc.: Stroudsbourg, PA, 1973.
(4) Selye, H. Adaptation Energy. *Nature* **1938**, *141*, 926.
(5) Selye, H. *The Stress of Life*; McGraw-Hill: New York, 1975.
(6) Moore-Ede, M. C. Physiology of the Circadian Timing System: Predictive versus Reactive Homeostasis. *Am. J. Physiol.* **1986**, *250*, R737−R752.
(7) Mrosovsky, N. *Rheostasis. The Physiology of Change*; Oxford University Press: New York, 1990.
(8) Bonny, O.; Firsov, D. Circadian Clock and the Concept of Homeostasis. *Cell Cycle* **2009**, *8*, 4015−4016.
(9) Sterling, P.; Eyer, J. In *Handbook of Life Stress, Cognition and Health*; Fisher, S., Reason, J., Eds.; John Wiley & Sons: New York, 1988; pp 629−649.
(10) Schulkin, J. *Rethinking Homeostasis. Allostatic Regulation in Physiology and Pathophysiology*; MIT Press: Cambridge, MA, 2003.
(11) Schulkin, J. *Allostasis, Homeostasis and the Costs of Physiological Adaptation*; Cambridge University Press: Cambridge, 2004.
(12) Lloyd, D.; Aon, M.; Cortassa, S. Why Homeodynamics, Not Homeostasis? *Sci. World J.* **2001**, *1*, 133−145.
(13) Wiener, N. *The Human Use of Human Beings*; Houghton Mifflin and Da Capo Press: Boston, 1954; Chapter V.
(14) Wiener, N. *Cybernetics: or Control and Communication in the Animal and the Machine*, 2nd ed.; The MIT Press: Cambridge, MA, 1961.
(15) Wilkie, J.; Johnson, M.; Reza, K. *Control Engineering. An Introductory Course*; Palgrave: New York, 2002.
(16) Hughes, G. M. *Homeostasis and Feedback Mechanisms*; Academic Press: New York, 1964.
(17) Drengstig, T.; Jolma, I.; Ni, X.; Thorsen, K.; Xu, X.; Ruoff, P. A Basic Set of Homeostatic Controller Motifs. *Biophys. J.* **2012**, *103*, 2000−2010.
(18) Yi, T. M.; Huang, Y.; Simon, M. I.; Doyle, J. Robust Perfect Adaptation in Bacterial Chemotaxis through Integral Feedback Control. *Proc. Natl. Acad. Sci. U.S.A.* **2000**, *97*, 4649−4653.
(19) El-Samad, H.; Goff, J.; Khammash, M. Calcium Homeostasis and Parturient Hypocalcemia: An Integral Feedback Perspective. *J. Theor. Biol.* **2002**, *214*, 17−29.
(20) Ang, J.; Bagh, S.; Ingalls, B.; McMillen, D. Considerations for Using Integral Feedback Control to Construct a Perfectly Adapting Synthetic Gene Network. *J. Theor. Biol.* **2010**, *266*, 723−738.
(21) Ang, J.; McMillen, D. Physical Constraints on Biological Integral Control Design for Homeostasis and Sensory Adaptation. *Biophys. J.* **2013**, *104*, 505−515.
(22) Ni, X.; Drengstig, T.; Ruoff, P. The Control of the Controller: Molecular Mechanisms for Robust Perfect Adaptation and Temperature Compensation. *Biophys. J.* **2009**, *97*, 1244−1253.
(23) Jolma, I. W.; Ni, X. Y.; Rensing, L.; Ruoff, P. Harmonic Oscillations in Homeostatic Controllers: Dynamics of the p53 Regulatory System. *Biophys. J.* **2010**, *98*, 743−752.
(24) Drengstig, T.; Ni, X.; Thorsen, K.; Jolma, I.; Ruoff, P. Robust Adaptation and Homeostasis by Autocatalysis. *J. Phys. Chem. B* **2012**, *116*, 5355−5363.
(25) Thorsen, K.; Drengstig, T.; Ruoff, P. In *Control Theoretic Properties of Physiological Controller Motifs*, ICSSE 2013, IEEE International Conference on System Science and Engineering; IEEE: Budapest, 2013; pp 165−170.
(26) Thorsen, K.; Agafonov, O.; Selstø, C. H.; Jolma, I. W.; Ni, X. Y.; Drengstig, T.; Ruoff, P. Robust Concentration and Frequency Control in Oscillatory Homeostats. *PLoS One* **2014**, *9*, No. e107766.
(27) Thorsen, K.; Drengstig, T.; Ruoff, P. Transepithelial Glucose Transport and Na^+/K^+ Homeostasis in Enterocytes: An Integrative Model. *Am. J. Physiol.: Cell Physiol.* **2014**, *307*, C320−C337.
(28) Agafonov, O.; Selstø, C. H.; Thorsen, K.; Xu, X. M.; Drengstig, T.; Ruoff, P. The Organization of Controller Motifs Leading to Robust Plant Iron Homeostasis. *PLoS One* **2016**, *11*, No. e0147120.
(29) Larbat, R.; Robin, C.; Lillo, C.; Drengstig, T.; Ruoff, P. Modeling the Diversion of Primary Carbon Flux into Secondary Metabolism under Variable Nitrate and Light/Dark Conditions. *J. Theor. Biol.* **2016**, *402*, 144−157.
(30) Saunders, P. T.; Koeslag, J. H.; Wessels, J. A. Integral Rein Control in Physiology. *J. Theor. Biol.* **1998**, *194*, 163−173.
(31) Solé, R.; Goodwin, B. *How Complexity Pervades Biology*; Basic Books, 2000; Chapter 4.
(32) Cook, G. M.; Morgan, H. W. Hyperbolic Growth of Thermoanaerobacter thermohydrosulfuricus (Clostridium thermohydrosulfuricum) Increases Ethanol Production in pH-Controlled Batch Culture. *Appl. Microbiol. Biotechnol.* **1994**, *41*, 84−89.
(33) Eigen, M.; Biebricher, C. K.; Gebinoga, M.; Gardiner, W. C. The Hypercycle. Coupling of RNA and Protein Biosynthesis in the Infection Cycle of an RNA Bacteriophage. *Biochemistry* **1991**, *30*, 11005−11018.
(34) Khaled, A. R.; Durum, S. K. Lymphocide: Cytokines and the Control of Lymphoid Homeostasis. *Nat. Rev. Immunol.* **2002**, *2*, 817−830.
(35) Radhakrishnan, K.; Hindmarsh, A. *Description and Use of LSODE, the Livermore Solver for Ordinary Differential Equations*. NASA Reference Publication 1327, Lawrence Livermore National Laboratory Report UCRL-ID-113855.; National Aeronautics and Space Administration, Lewis Research Center: Cleveland, OH, 1993.
(36) Goodwin, B. *Temporal Organization in Cells*; Academic Press: London, 1963.
(37) Goodwin, B. *Advances in Enzyme Regulation*; Weber, G., Ed.; Pergamon Press: Oxford, U.K., 1965; Vol. 3, pp 425−438.
(38) Goodwin, B. Temporal Organization and Disorganization in Organisms. *Chronobiol. Int.* **1997**, *14*, 531−536.
(39) Gonze, D.; Abou-Jaoudé, W. The Goodwin Model: Behind the Hill Function. *PLoS One* **2013**, *8*, No. e69573.
(40) Francis, B. A.; Wonham, W. M. The Internal Model Principle of Control Theory. *Automatica* **1976**, *12*, 457−465.
(41) Isidori, A.; Byrnes, C. I. Output Regulation of Nonlinear Systems. *IEEE Trans. Autom. Control* **1990**, *35*, 131−140.
(42) Sontag, E. D. Adaptation and Regulation with Signal Detection Implies Internal Model. *Syst. Control Lett.* **2003**, *50*, 119−126.
(43) Selye, H. Experimental Evidence Supporting the Conception of "Adaptation Energy". *Am. J. Physiol.* **1938**, *123*, 758−765.
(44) Gorban, A. N.; Tyukina, T. A.; Smirnova, E. V.; Pokidysheva, L. I. Evolution of Adaptation Mechanisms: Adaptation Energy, Stress, and Oscillating Death. *J. Theor. Biol.* **2016**, 127.

DOI: 10.1021/acs.jpcb.7b01989
J. Phys. Chem. B 2017, 121, 6097−6107